Eur. Phys. J. AP **18**, 125–133 (2002)
DOI: 10.1051/epjap:2002034

THE EUROPEAN PHYSICAL JOURNAL APPLIED PHYSICS

Numerical simulation of an RF inductively coupled plasma for functional enhancement by seeding vaporized alkali metal

H. Nishiyama[a] and M. Shigeta[b]

Institute of Fluid Science, Tohoku University, 2-1-1, Katahira, Aoba-ku, Sendai, 980-8577, Japan

Received: 16 August 2001 / Received in final form: 4 December 2001 / Accepted: 7 January 2002

Abstract. The functions of the plasma flow such as electrical conductivity, thermal conduction and chemical reaction can be enhanced by seeding vaporized alkali metal with low ionization potential. In the present study, numerical simulation is conducted for the radio frequency inductively coupled plasma of which functions are enhanced by seeding a small amount of vaporized alkali metal. The effects of seeding, injection flow rate and applied coil frequency on the plasma characteristics are clarified by relating to the flow structure and electromagnetic effect.

PACS. 52.30.Cv Magnetohydrodynamics (including electron magnetohydrodynamics) – 52.65.Kj Magnetohydrodynamic and fluid equation – 52.80.Pi High-frequency and RF discharges

Nomenclature

$\mathbf{A}$: vector potential ($= (A_r, A_\theta, A_z)$) (A H m^{-1})
c : mean value of the thermal velocity (m)
C_n : mole fraction
C_p : specific heat at constant pressure (J kg^{-1} K^{-1})
D : diffusion coefficient (m^2 s^{-1})
D_{amb}: ambipolar diffusion coefficient (m^2 s^{-1})
e : electron charge (C)
$\mathbf{E}$: electric field vector ($= (E_r, E_\theta, E_z)$) (V m^{-1})
f : frequency (Hz)
$\mathbf{F}$: Lorentz force vector ($= (F_r, F_\theta, F_z)$) (N m^{-3})
h : enthalpy (J kg^{-1})
$\mathbf{H}$: magnetic field vector ($= (H_r, H_\theta, H_z)$) (A m^{-1})
I : coil current (A)
k : Boltzmann constant (J K^{-1})
k_{eq} : equilibrium constant (m^{-3})
k_{ion} : ionization coefficient (m^3 s)
k_{re} : recombination coefficient (m^6 s^{-1})
l : mean free path (m)
m : mass (kg)
n : number density (m^{-3})
p : pressure (Pa)
P : coil input power (kW)
Q : flow rate (Sl min^{-1})
$\overline{Q}$: collision cross section (m^{-2})
Q_j : Joule heating (J m^{-3})
Q_r : radiation loss (J m^{-3})
r : radial coordinate (m)
r_1 : carrier gas nozzle radius (m)
r_2 : plasma gas nozzle radius (m)
T : temperature (K)
u : velocity component in axial direction (m s^{-1})
v : velocity component in radial direction (m s^{-1})
w : velocity component in azimuthal direction (m s^{-1})
w_{R}: swirl ratio ($= w\, r_W / u\, r$)
z : axial coordinate (m)

Greek symbols

ε_0 : permittivity in vacuum (F m^{-1})
η : viscosity (Pa s)
θ : azimuthal coordinate (m)
λ : thermal conductivity (W m^{-1} K^{-1})
μ_0 : permeability in vacuum (H/m)
δ : skin depth (m)
μ : mobility
ρ : density (kg m^{-3})
σ : electrical conductivity (S m^{-1})

[a] e-mail: nishiyama@ifs.tohoku.ac.jp
[b] e-mail: shigeta@paris.ifs.tohoku.ac.jp

Subscripts

Ar	: argon atom
Ar^+	: argon ion
s	: seed atom
s^+	: seed ion
e	: electron
h	: heavy particles
R	: real part
I	: imaginary part
C	: coil
W	: wall
r	: radial component
z	: axial component
θ	: azimuthal component

1 Introduction

Plasma can be regarded as one of the multifunctional fluids [1] since it has high energy density, chemical reactivity and variable transport properties such as electrical conductivity. Furthermore, plasma can be easily controlled by applying an electromagnetic field. In the various kinds of plasma, a radio frequency inductively coupled plasma (RF-ICP) has advantages of large volume, clean high energy and chemical reactivity since it is produced without electrodes. Furthermore, the chemical reaction time is comparatively long due to the low plasma velocity. It has, therefore, been extensively used in the reactive plasma spraying, synthesis of ultrafine powders and decomposition of hazardous substances such as fleon and dioxin, for example. In these industrial applications, it is very important to enhance the functions of plasma and control them precisely [2–5]. It is well known that seeding a small amount of vaporized alkali metal with low ionization potential into plasma is one of effective methods for the enhancement of the functions of plasma such as electrical conductivity [6]. When a small amount of alkali metals is seeded to produce many electrons actively, plasma controllability can be also enhanced by utilizing Lorentz force and Joule heating with increase in the electrical and thermal conductivities. There have, however, been a few theoretical papers clearing with the enhancement of the functions of plasma by seeding alkali metals [7,8].

In the present study, it is numerically investigated how its functions and thermofluid characteristics of the RF inductively coupled argon plasma are influenced and enhanced by seeding vapor potassium or cesium at atmospheric pressure taking into account the ionization, recombination and diffusion of each plasma species. The effects of gas injection flow rate and applied frequency on the RF argon plasma with seeding are also clarified to extend the enhanced ICP in the industrial applications relating to the flow structure and the electromagnetic effect.

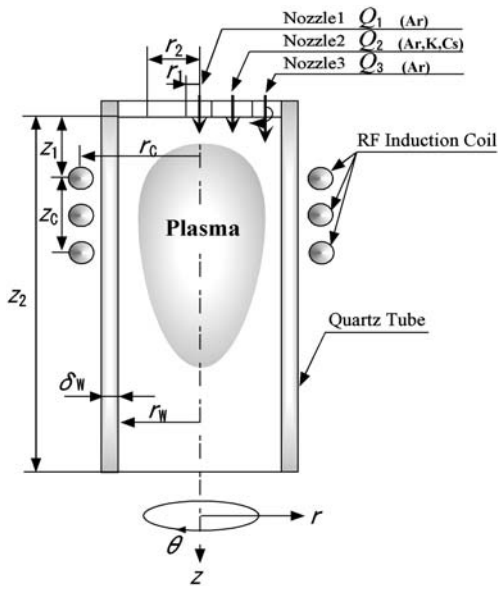

Fig. 1. Schematic illustration of the RF-ICP torch with seeding.

2 Numerical model

2.1 Governing equations

A schematic illustration of the RF-ICP torch is shown in Figure 1. The inlet portion has three nozzles for carrier gas, plasma gas and sheath gas respectively. An RF-ICP is produced and maintained in the torch by the RF induction coils (3–13.56 MHz, 8 kW). The seed materials are prevaporized and injected into the plasma gas through the nozzle 2 as a plasma gas.

The plasma model is proposed on the following assumptions:

- steady, laminar and 2D axisymmetric flow and temperature fields
- 2D axisymmetric induction electromagnetic fields with negligible displacement currents
- negligible gravitational forces and viscous dissipation
- local thermal equilibrium (LTE) and optically thin
- two-body collision ionization and three-body recombination
- ambipolar diffusion of ions and electrons.

There are some papers about the deviation of LTE especially under the low operating pressure or near wall in the coil region where the temperature gradient is steep in RF- ICP [9]. But the hypothesis of LTE or close-to-LTE is considered to be valid for an RF- ICP operated at atmospheric pressure and at a coil frequency of a few MHz.

The governing equations of continuity, momentum, energy, and plasma species per unit volume are summarized in the following general form in cylindrical coordinates:

$$\frac{\partial}{\partial z}(\psi u\phi) + \frac{1}{r}\frac{\partial}{\partial r}(r\psi v\phi) = \frac{\partial}{\partial z}\left(\Gamma\frac{\partial\phi}{\partial z}\right) + \frac{1}{r}\frac{\partial}{\partial r}\left(r\Gamma\frac{\partial\phi}{\partial r}\right) + S \quad (1)$$

Table 1. Transport coefficients and the source terms for the governing equations (1).

ϕ	ψ	Γ	S
1	ρ	0	0
u	ρ	η	$-\frac{\partial p}{\partial z}+\frac{\partial}{\partial z}\left(\eta\frac{\partial u}{\partial z}\right)+\frac{1}{r}\frac{\partial}{\partial r}\left(r\eta\frac{\partial v}{\partial z}\right)$ $-\frac{2}{3}\frac{\partial}{\partial z}\left(\eta\left(\frac{\partial u}{\partial z}+\frac{1}{r}\frac{\partial (rv)}{\partial r}\right)\right)-\frac{1}{2}\mu_0\sigma Real\left(E_\theta \overline{H}_r\right)$
v	ρ	η	$-\frac{\partial p}{\partial r}+\frac{\partial}{\partial z}\left(\eta\frac{\partial u}{\partial r}\right)+\frac{1}{r}\frac{\partial}{\partial r}\left(r\eta\frac{\partial v}{\partial r}\right)-\frac{2}{3}\frac{\partial}{\partial r}\left(\eta\left(\frac{\partial u}{\partial z}+\frac{1}{r}\frac{\partial (rv)}{\partial r}\right)\right)$ $-\eta\frac{2v}{r^2}+\rho\frac{w^2}{r}+\frac{1}{2}\mu_0\sigma Real\left(E_\theta \overline{H}_z\right)$
w	ρ	η	$-\frac{w}{r^2}\frac{\partial}{\partial r}(r\eta)-\rho\frac{vw}{r}$
h	ρ	λ / C_p	$\frac{1}{2}\sigma E_\theta \overline{E}_\theta - Q_r$
n_{Ar^+}	1	$D_{Ar^+ amb}$	$k_{Ar\,ion}n_{Ar}n_e - k_{Ar\,re}n_{Ar^+}{n_e}^2$
n_{s^+}	1	$D_{s^+ amb}$	$k_{s\,ion}n_s n_e - k_{s\,re}n_{s^+}{n_e}^2$
n_s	1	D_s	$k_{s\,re}n_{s^+}{n_e}^2 - k_{s\,ion}n_s n_e$

Table 1 shows the transport coefficients and the source terms in the governing equations for the plasma flow.

Since plasma is assumed to be electrically neutral, the electron number density is written as

$$n_\mathrm{e} = n_{\mathrm{Ar}^+} + n_{\mathrm{s}^+} \tag{2}$$

The governing equation of the induction electromagnetic fields is expressed as

$$\frac{\partial^2 A_\theta}{\partial z^2}+\frac{1}{r}\frac{\partial}{\partial r}\left(r\frac{\partial A_\theta}{\partial r}\right)-\frac{A_\theta}{r^2}=i\mu_0\sigma\omega A_\theta \tag{3}$$

where i is equal to $\sqrt{-1}$. The induction electromagnetic fields are represented using the electromagnetic vector potential for solving a 2D induction electromagnetic field equation to consider the interaction between the applied electromagnetic field of the coils and the induction electromagnetic field of the plasma. For a standard induction plasma torch with the coil geometry shown in Figure 1, it is reasonable to assume that the electromagnetic field, and thus the vector potential, has only a azimuthal component. Then the induction electromagnetic fields are given by Maxwell's equations.

$$E_\theta = -i\omega A_\theta \tag{4}$$

$$\mu_0 H_z = \frac{1}{r}\frac{\partial (rA_\theta)}{\partial r} \tag{5}$$

$$\mu_0 H_r = -\frac{\partial A_\theta}{\partial z} \tag{6}$$

2.2 Thermodynamic and transport properties

In this paper, it is reasonable that the thermal conductivity and viscosity are separated into the contribution from heavy particles and electrons, and written as

$$\lambda = \lambda_\mathrm{h} + \lambda_\mathrm{e} \tag{7}$$

$$\eta = \eta_\mathrm{h} + \eta_\mathrm{e} \tag{8}$$

since the increase in electron number density by seeding alkali metal affects the transport properties considerably. λ_h and η_h are calculated from the database of only argon [11] neglecting the small seed fraction of heavy particles of alkali metal. λ_e and η_e are given from the kinetic theory as [12]

$$\lambda_\mathrm{e} = \frac{75\pi}{128}n_\mathrm{e}kl_\mathrm{e}c_\mathrm{e} \tag{9}$$

$$\eta_\mathrm{e} = \frac{5\pi}{32}m_\mathrm{e}n_\mathrm{e}l_\mathrm{e}c_\mathrm{e} \tag{10}$$

where l_e and c_e are the mean free path and the mean value of the thermal velocity of electrons respectively.

Since the electrical conductivity is expected to be remarkably enhanced with increase in electron number density by seeding a small amount of vaporized alkali metal, it is given as a function of electron number density.

$$\sigma = \frac{e^2 n_\mathrm{e}}{m_\mathrm{e}(c_\mathrm{e}/l_\mathrm{e})} \tag{11}$$

Diffusion coefficient of the seed atom in argon gas is written approximately as

$$D_\mathrm{s} = \frac{\eta}{\rho Sc} \tag{12}$$

where Schmidt number Sc is 1.0 here. Ambipolar diffusion

coefficient of the heavy particle ion is given by

$$D_{\mathrm{h}^+\,\mathrm{amb}} = \frac{\mu_\mathrm{e} D_{\mathrm{h}^+} + \mu_{\mathrm{h}^+} D_\mathrm{e}}{\mu_\mathrm{e} + \mu_{\mathrm{h}^+}} \qquad \left(\mathrm{h}^+ = \mathrm{Ar}^+, \mathrm{s}^+\right) \quad (13)$$

where μ_e and μ_{h^+} are mobilities of electron and heavy particle ion respectively. On the other hand, diffusion coefficients of electron and heavy particle ion are given respectively by

$$D_\mathrm{e} = \frac{kT_\mathrm{e}}{m_\mathrm{e}(c_\mathrm{e}/l_\mathrm{e})} \quad (14)$$

$$D_{\mathrm{h}^+} = \frac{kT}{m_{\mathrm{h}^+}(c_{\mathrm{h}^+}/l_{\mathrm{h}^+})} \qquad \left(\mathrm{h}^+ = \mathrm{Ar}^+, \mathrm{s}^+\right) \quad (15)$$

where l_{h^+} and c_{h^+} are the mean free path and the mean value of the thermal velocity of heavy particle ions respectively. To calculate the mean free paths, collision cross sections are used. Collision cross sections $\overline{Q}_{\mathrm{ArAr}}$, $\overline{Q}_{\mathrm{Ar^+Ar^+}}$, $\overline{Q}_{\mathrm{Ar^+Ar}}$ and $\overline{Q}_{\mathrm{eAr}}$ are given by the multiple terms approximation as a function of temperature from the experimental data [13]; $\overline{Q}_{\mathrm{eK}}$ and $\overline{Q}_{\mathrm{eCs}}$ are also given from the data [14]; Coulomb cross section $\overline{Q}_{\mathrm{eh}^+}$ is expressed

$$\overline{Q}_{\mathrm{eh}^+} = 6\pi \left(\frac{e^2}{12\pi\varepsilon_0 kT_\mathrm{e}}\right)^2 \ln\left\{\frac{9\left(4\pi\varepsilon_0 kT_\mathrm{e}\right)^3}{4\pi n_\mathrm{e} e^6}\right\}^{\frac{1}{2}} \qquad \left(\mathrm{h}^+ = \mathrm{Ar}^+, \mathrm{s}^+\right) \quad (16)$$

Since the exact data of the collision cross section between argon and alkali metal are not available, they can be assumed as follows in the present study corresponding to Coulomb collisional section effect and the diameters of the heavy particles respectively.

$$\overline{Q}_{\mathrm{Ar^+s^+}} = \overline{Q}_{\mathrm{Ar^+Ar^+}} \quad (17)$$

$$\overline{Q}_{\mathrm{Ars^+}} = \frac{\overline{Q}_{\mathrm{es}}}{\overline{Q}_{\mathrm{eAr}}} \overline{Q}_{\mathrm{ArAr^+}} \quad (18)$$

The density, the specific heat at constant pressure and the radiation loss of the argon-alkali metal mixed plasma are replaced with those of the argon plasma since the seed fraction is small in the present study [10,11].

The recombination coefficients k_re of argon and alkali metals are taken from [15–17]. The ionization coefficient k_ion is expressed

$$k_\mathrm{ion} = k_\mathrm{eq} \cdot k_\mathrm{re} \quad (19)$$

where the equilibrium coefficient k_eq is estimated by Saha's equation.

2.3 Boundary conditions

The boundary conditions to determine the flow, temperature, concentration and electromagnetic fields are described without considering the recombination and the plasma sheath on the wall since the sheath depth is the order of Debye length which is considerably smaller compared with plasma diameter [1,3]. Non-slip condition, thermal conduction and electrical insulation are taken into account at the inner surface of the tube. For the vector potential at the wall, the contributions of both the coil currents and the induced currents in the plasma are taken into account [18]. Since vector potential A_θ is complex, it is divided into the real part A_R and the imaginary part A_I in the present simulation.

Inlet ($z = 0$)

$$u = \begin{cases} Q_1/\pi r_1^2 & 0 \le r < r_1 \\ Q_2/\pi(r_2^2 - r_1^2) & r_1 \le r < r_2 \\ Q_3/\pi(r_W^2 - r_2^2) & r_2 \le r < r_W \end{cases}$$

$$v = 0$$

$$w = \begin{cases} 0 & 0 \le r < r_1 \\ 0 & r_1 \le r < r_2 \\ w_\mathrm{R} u(r/r_W) & r_2 \le r < r_W \end{cases}$$

$$T_\mathrm{in} = 800 \text{ (K)}$$

$$n_\mathrm{s} = \begin{cases} 0 & 0 \le r < r_1 \\ C_{ns} p/kT_\mathrm{in} & r_1 \le r < r_2 \\ 0 & r_2 \le r < r_W \end{cases}$$

$$n_{\mathrm{Ar}^+} = 0$$

$$n_{\mathrm{s}^+} = 0$$

$$\frac{\partial^2 A_\mathrm{R}}{\partial z^2} = \frac{\partial^2 A_\mathrm{I}}{\partial z^2} = 0$$

Axis ($r = 0$)

$$\frac{\partial u}{\partial r} = v = w = 0$$

$$\frac{\partial T}{\partial r} = \frac{\partial n_\mathrm{s}}{\partial r} = \frac{\partial n_{\mathrm{Ar}^+}}{\partial r} = \frac{\partial n_{\mathrm{s}^+}}{\partial r} = 0$$

$$A_\mathrm{R} = A_\mathrm{I} = 0$$

Table 2. Torch geometry and operating conditions.

Radius of nozzle1 r_1 (mm)	5.5
Radius of nozzle2 r_2 (mm)	17.0
Torch radius r_W (mm)	25.0
Coil radius r_C (mm)	33.0
Coil length z_C (mm)	20.0
Axial position of coil z_1 (mm)	30.0
Torch length z_2 (mm)	200.0
Wall thickness δ_W (mm)	5.0
Coil turn number N (turns)	3.0
Inlet temperature T_{in} (K)	800.0
Coil input power P (kW)	8.0
Coil frequency f (MHz)	3.0, 13.56
Operating pressure p (atm)	1.0
Seed fraction C_{ns} (-)	0.03

Wall ($r = r_W$)

$$u = v = w = 0$$

$$-\frac{\lambda}{C_p}\frac{\partial h}{\partial r} = \frac{\lambda_W}{\delta_W}\left(T - T_{\text{outer-wall}}\right)$$

$$T_{\text{outer-wall}} = 300 \text{ (K)}$$

$$\frac{\partial n_{\text{s}}}{\partial r} = \frac{\partial n_{\text{Ar}^+}}{\partial r} = \frac{\partial n_{\text{s}^+}}{\partial r} = 0$$

$$A_{\text{R}}(r_W, z) = \frac{\mu_0 I}{2\pi}\sqrt{\frac{r_C}{r_W}}\sum_{j=1}^{\text{coil}} G(l_j) + \frac{\mu_0 \omega}{2\pi}\sum_{j=1}^{\text{C.V.}}\sqrt{\frac{r_j}{r_W}}\sigma_j A_{I\text{j}} S_j G(l_j)$$

$$A_{\text{I}}(r_W, z) = -\frac{\mu_0 \omega}{2\pi}\sum_{j=1}^{\text{C.V.}}\sqrt{\frac{r_j}{r_W}}\sigma_j A_{R\text{j}} S_j G(l_j)$$

Outlet ($z = z_2$)

$$\frac{\partial^2(\rho u)}{\partial z^2} = \frac{\partial^2 v}{\partial z^2} = \frac{\partial^2 w}{\partial z^2} = 0$$

$$\frac{\partial^2 T}{\partial z^2} = \frac{\partial^2 n_{\text{s}}}{\partial z^2} = \frac{\partial^2 n_{\text{Ar}^+}}{\partial z^2} = \frac{\partial^2 n_{\text{s}^+}}{\partial z^2} = 0$$

$$\frac{\partial^2 A_{\text{R}}}{\partial z^2} = \frac{\partial^2 A_{\text{I}}}{\partial z^2} = 0$$

The inlet temperature T_{in} is set at 800 K, since the seed materials need to be prevaporized before injection. T_{w} of 300 K is the outer-surface temperature of the tube. $G(l_j)$ is a function of complete elliptic integrals and C.V. indicates control volume.

2.4 Numerical procedure

A summary of the torch geometry and the operating conditions in the present calculation is given in Table 2, with reference to a commercial RF induction coupled plasma torch. The prevaporized seed materials are injected from nozzle 2 as mixing with a plasma gas. The swirl ratio w_{R} is given 5.0 at the nozzle 3.

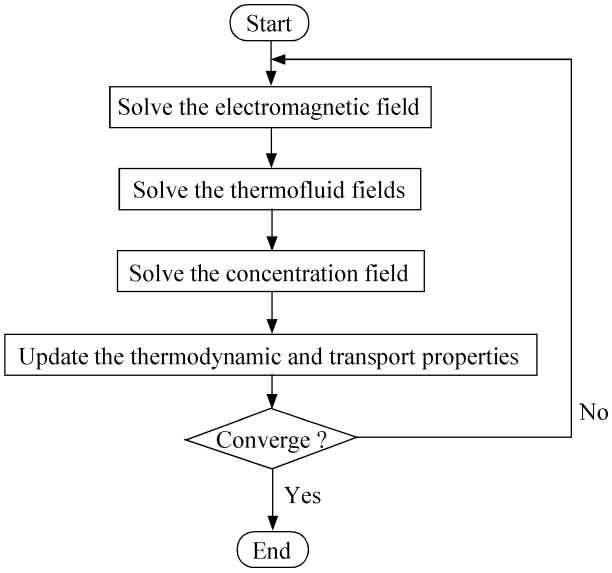

Fig. 2. Flow chart for the computational procedure.

The operating parameters are shown in Table 3. Case 1, Case 2 and Case 3 correspond to three cases without seeding, seeding potassium and seeding cesium respectively. In Case 4, the inlet flow rates Q_1, Q_2 and Q_3 are 10.0 Sl/min, 10.0 Sl/min and 25.0 Sl/min respectively and the seed material is potassium. In Case 5 and Case 6, the coil frequency f is 13.56 MHz without and with seeding respectively. The seed material is potassium in Case 6.

The governing equations for the velocity, temperature, concentration and electromagnetic fields, along with the boundary conditions, were solved using the SIMPLE algorithm developed by Patankar [19]. The simulations were performed for a 101 in r-direction by 101 in z-direction uniform staggered grid system to obtain the converged solutions easily.

Figure 2 shows the flow chart for the computational procedure. In the simulations, TDMA (Tri-Diagonal Matrix Algorithm) was used to solve the matrices. The residual 10^{-3} for the electromagnetic field, 10^{-6} for the thermofluid field and 10^{-4} for the concentration field were set up as the convergence criteria.

3 Results and discussion

3.1 Influence of seeding alkali metal

Figure 3 shows a comparison of the electron number density distributions in Cases 1-3. Although the electrons exist only near the coils in Case 1 without seeding, the electrons are diffused both to the central region and in the further downstream wider even by seeding a small amount of vaporized alkali metals such as potassium in Case 2 and cesium in Case 3.

Table 3. Operating parameters.

	Seed material	Inlet flow rate			Coil frequency
		Q_1(Sl/min)	Q_2(Sl/min)	Q_3(Sl/min)	f (MHz)
Case1	without seed	2.0	2.0	5.0	3.0
Case2	K	2.0	2.0	5.0	3.0
Case3	Cs	2.0	2.0	5.0	3.0
Case4	K	10.0	10.0	25.0	3.0
Case5	without seed	2.0	2.0	5.0	13.56
Case6	K	2.0	2.0	5.0	13.56

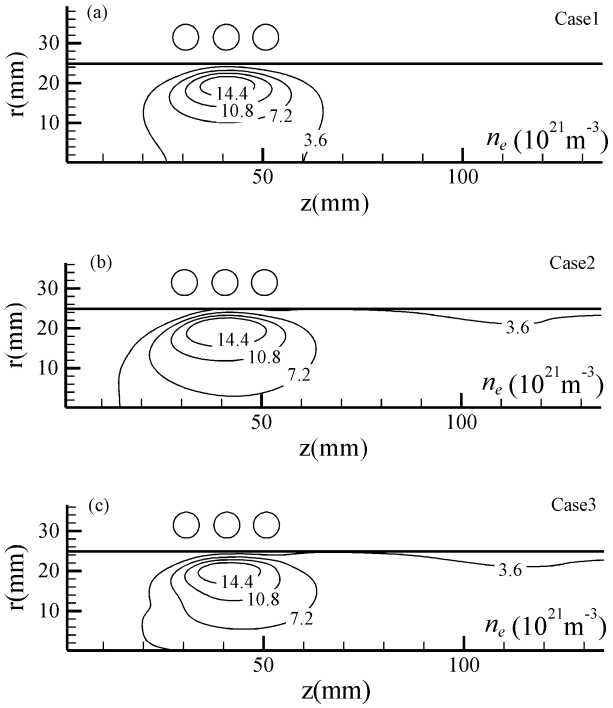

Fig. 3. (a)-(c) Electron number density distributions.

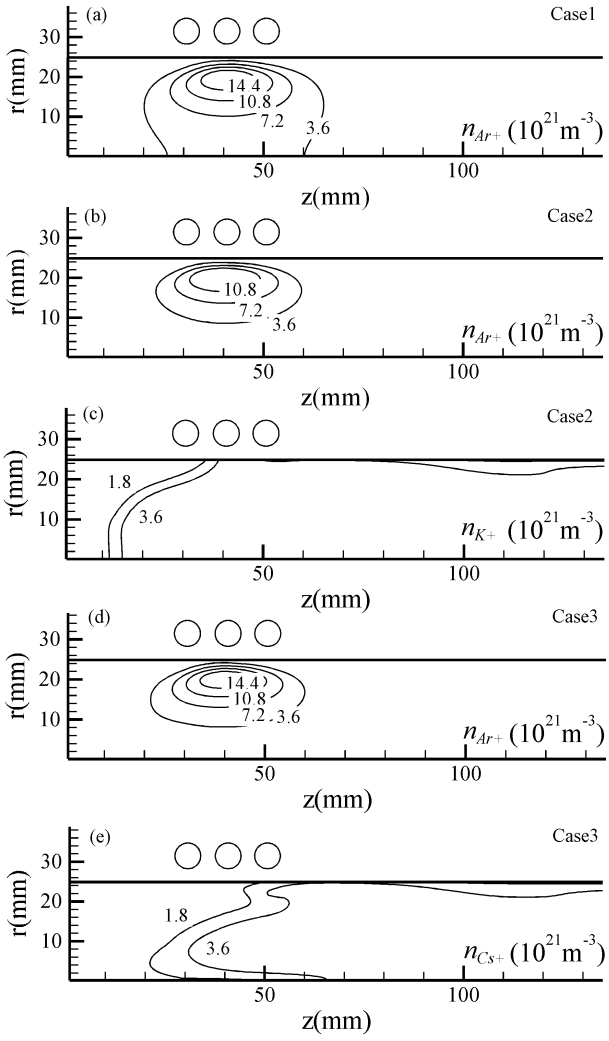

Fig. 4. (a)-(e) Ion number density distributions.

Figure 4 shows a comparison of the corresponding argon ion, potassium ion and cesium ion number densities distributions in Cases 1-3. It is clearly shown that the vaporized alkali metals can be ionized easily at the region of lower temperature compared with argon ionization. The difference between the distributions in Case 2 and in Case 3 are caused by the difference of heavy particle ions diffusion. The electrons and ions diffuse together and also the cesium ions may be dominated by convection more than potassium ions since the diffusion coefficient of cesium ions is smaller than that of potassium ions due to the large mass.

Figure 5 shows a comparison of the electrical conductivity distributions in Cases 1-3. The electrical conductivity, one of the functions of plasma, in seeding alkali metals increases considerably in the coil just downstream accompanied by the increase in electrons as shown in Figure 3. This means that the electrical conductivity as a function of plasma is enhanced by seeding vaporized alkali metals and then the region where is influenced by the applied electromagnetic fields becomes wider in the downstream. As the result, that can affect Joule heating and temperature field.

Figure 6 shows a comparison of the temperature distribution in Cases 1-3. In Case 2 and Case 3, seeding alkali metals enhance the function of the plasma and then the region of temperature 2000–6000 K shifts to the further downstream compared with that in Case 1.

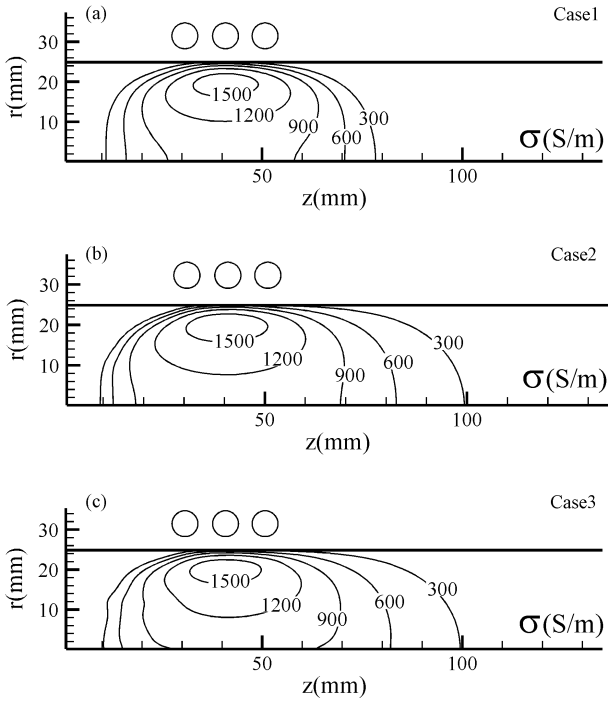

Fig. 5. (a)-(c) Electrical conductivity distributions.

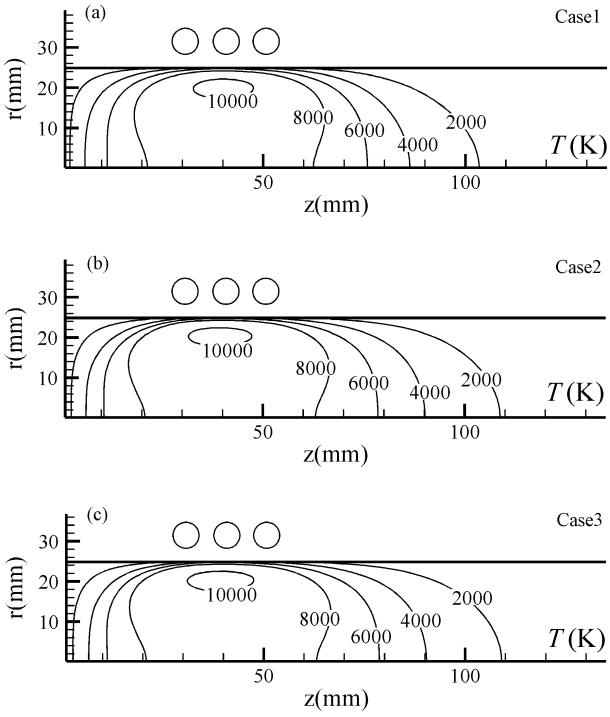

Fig. 6. (a)-(c) Temperature distributions.

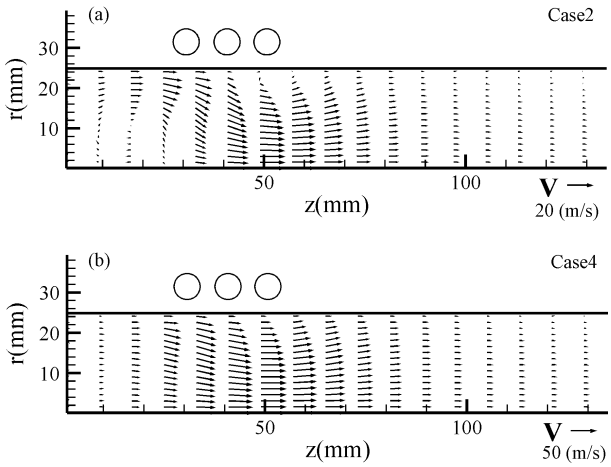

Fig. 7. (a)-(b) Velocity vector distributions.

3.2 Influence of inlet flow rate

Figure 7 shows a comparison of the velocity vector distributions in Case 2 and Case 4 with potassium seeding. Circulation is produced by Lorentz force and inlet flow rate difference. In Case 2, the flow field has a circulating region near the coil region. This is because the radial Lorentz force is produced by the induction electromagnetic fields in the plasma, which pinch the flow field of the plasma. On the other hand, in Case 4, the circulating region disappears with the higher inlet flow rate in spite of the pinch effect of the Lorentz forces since the inertia force overcomes the Lorentz force with the increase in the inlet flow rate. When the flow rate is lower compared with Case 1 or 2, strong vortices are observed near the central region.

3.3 Influence of coil frequency

Figure 8 shows a comparison of the electrical conductivity distributions in Case 1, Case 5 and Case 6. When the applied coil frequency is high, the maximum region of the electrical conductivity approaches to the wall in both cases compared with Case 1 due to the skin effect which is closely related to skin depth defined by $\delta = (2\pi\mu_0\sigma f)^{-\frac{1}{2}}$. By seeding potassium in Case 6, the region of the high electrical conductivity extends to the further downstream considerably and the electrical conduction is enhanced.

Figure 9 shows a comparison of the Joule heating distribution in Case 1, Case 5 and Case 6. In both cases, the high Joule heating regions show the flat distribution near the wall compared with Case 1 as well as the distributions of the electrical conductivity in Figure 8 since the skin depth becomes thinner when the applied coil frequency is high. The high Joule heating region in Case 6 shows the thinner distribution near the wall compared with that in Case 5 because the electrical conduction is enhanced by seeding potassium as shown Figure 8 and the applied electromagnetic fields are absorbed in plasma near the wall more than in Case 5.

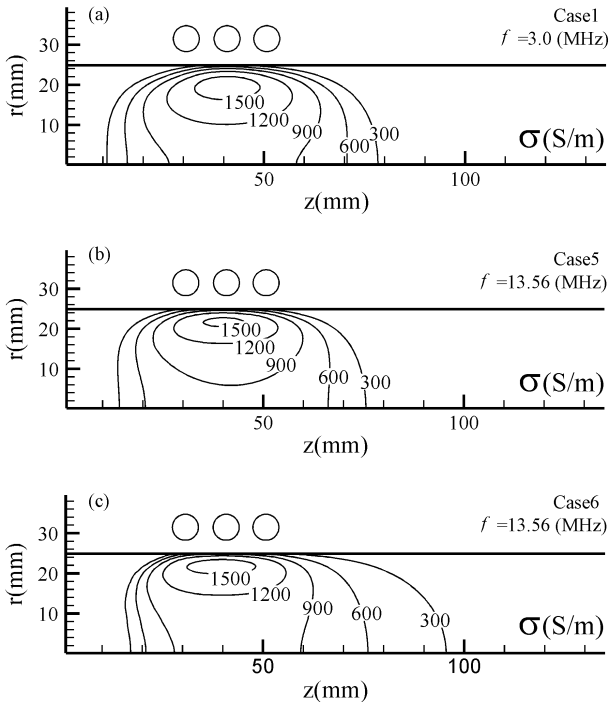

Fig. 8. (a)-(c) Electrical conductivity distributions.

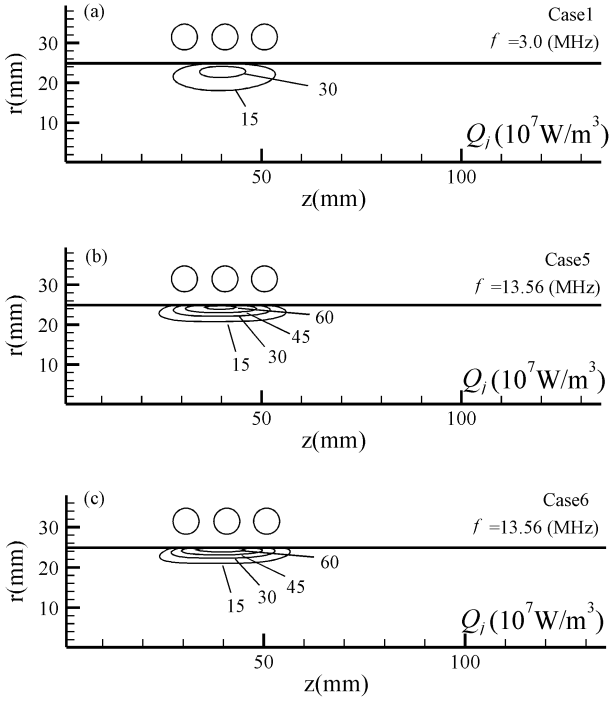

Fig. 9. (a)-(c) Joule heating distributions.

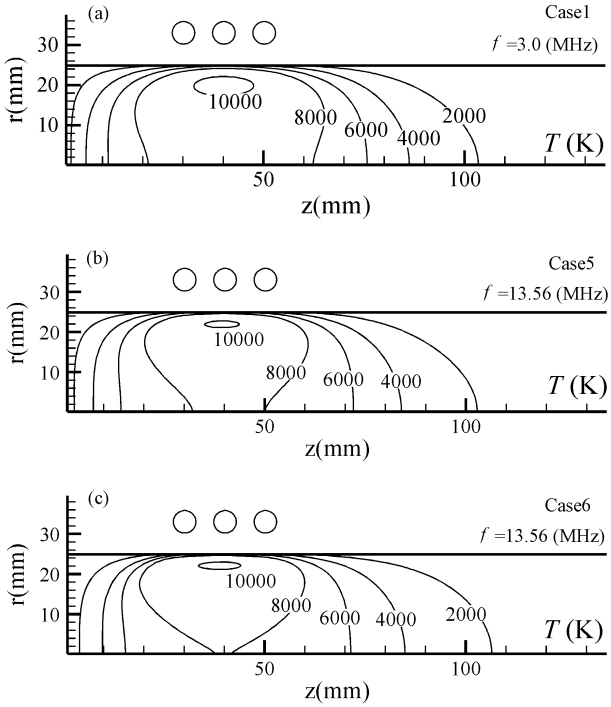

Fig. 10. (a)-(c) Temperature distributions.

Figure 10 shows a comparison of the temperature distribution in Case 1, Case 5 and Case 6. In both Case 5 and Case 6, the high temperature regions more than 8000 K become narrower compared with Case 1 due to the concentration of the Joule heating with the skin effect as shown in Figure 9. Especially in Case 6, since the electrical conduction is enhanced by seeding vaporized alkali metal, the region of the temperature higher than 8000 K becomes narrower and closer to the wall than in Case 5. The region of the temperature 2000–6000 K in Case 6, however, is relatively wider further downstream compared with that in Case 5. As the result, it can be shown that it is possible to control the temperature field of the RF-ICP relatively and that seeding alkali metal is effective to enhance the electrical conduction and the controllability of the RF-ICP for high frequency.

Figure 11 shows a comparison of the velocity vector distribution in Case 5 and Case 6. Since the Lorentz forces do not penetrate into the central region of the plasma by the skin effect for high frequency in both cases, the recirculating region, which is seen in Case 2, disappears with the increase in the applied coil frequency. As the result, it is possible to produce or eliminate recirculating regions and control the flow field of the RF-ICP by changing the applied coil frequency.

The effect of the applied frequency on the thermofluid field of RF-ICP can be enhanced by seeding even a small amount of alkali metal vapor.

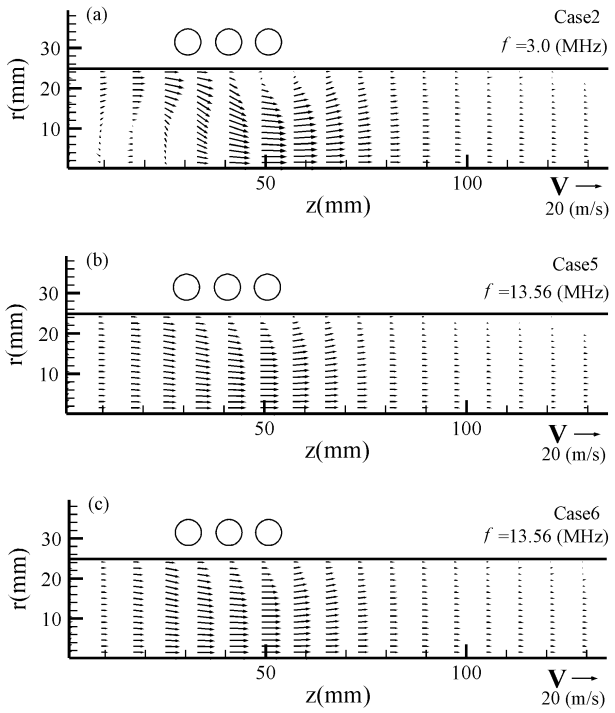

Fig. 11. (a)-(c) Velocity vector distributions.

4 Conclusion

It is investigated how functions and thermofluid characteristics of the RF inductively coupled argon plasma are influenced and enhanced by seeding vapor potassium or cesium at atmospheric pressure taking the ionization, recombination and diffusion of the plasma species into account. It is found that almost the same qualitative tendency can be shown as the several works using this model [2, 7]. The results obtained by numerical simulation are as follows.

1. The electron number density increases and the electrons are distributed wider in the further downstream by seeding alkali metals. Then, the high electrical conductivity region extends to the downstream with the increase in the electrons. The distributions of the electron number density and the electrical conductivity in seeding potassium and cesium are different due to the difference of their diffusion coefficient. The region of temperature of 2000–6000 K becomes wider in the downstream. Seeding alkali metals affects locally the functions such as the electrical conduction and the temperature field.
2. The flow field has a recirculating region caused by the radial Lorentz forces. The recirculating region near the coil region disappears with the high inlet flow rate which overcomes the Lorentzian pinch effect.
3. When the applied coil frequency increases, the Joule heating concentrates near the wall by the skin effect. As the result, the high electrical conductivity region approaches the wall and the high temperature region more than 8000 K becomes thinner and closer to the wall. With the increase of the applied coil frequency, the Lorentz force also concentrates near the wall and then vortices disappear in the coil region. It is easily possible to control the temperature field and the flow field of the RF-ICP by changing the applied coil frequency especially under the condition of seeding a small amount of alkali metal vapor.

This work was partly supported by a grant-in-aid for Scientific Research (B) from the Japan Society for Promotion of Science (2001). This numerical simulation was performed using an Origin2000 at the Super Computer Center of the Institute of Fluid Science, Tohoku University, Japan.

References

1. Japan Society of Mechanical Engineers, *Functional Fluids and Intelligent Fluids* (Corona Pub. Corp., Japan, 2000).
2. H. Nishiyama, T. Sato, A. Veefkind, S. Kamiyama, Heat Mass Transfer **30**, 291 (1995).
3. H. Nishiyama, Y. Muro, S. Kamiyama, J. Phys. D: Appl. Phys. **29**, 2634 (1996).
4. H. Nishiyama, N. Fukai, S. Kamiyama, JSME Int. J. Ser. B **41**, 502 (1998).
5. R.J. Rosa, *Magnetohydrodynamic Energy Conversion Rev.* (Hemisphere, New York, 1987).
6. J.H. Park, S.H. Hong, IEEE Trans. Plasma Sci. **23**, 532 (1995).
7. T. Suekane, T. Taya, Y. Okuno, S. Kabashima, IEEE Trans. Plasma Sci. **24**, 1147 (1996).
8. M. Shigeta, H. Nishiyama, *Proc. 15th Int. Symp. on Plasma Chemistry, 2001*, Vol. III, p. 1209.
9. D.V. Gravelle, M. Beaulieu, M.I. Boulos, A. Gleizes, J. Phys. D: Appl. Phys. **22**, 1471 (1989).
10. J. Menart, H. Lin, J. Thermophys. Heat Transfer **12**, 500 (1998).
11. M.I. Boulos, P. Fauchais, E. Pfender, *Thermal Plasma* (Plenum Press, New York, 1994), Vol. 1.
12. L.E. Kalikhman, *Elements of Magnetogasdynamics* (Saunders, Philadelphia, 1967).
13. J. Kanzawa, *Plasma Heat Transfer* (Shinzan Corp., Japan, 1992).
14. F.E. Spencer, A.V. Phelps, in *Proceedings of 15th Symposium Engineering Aspects of MHD, 1976*, Vol. IX, p. 9.1.
15. M.I. Hoffert, H. Lien, Phys. Fluids **10**, 1769 (1967).
16. E. Hinnov, J.G. Hirschberg, Phys. Rev. **125**, 795 (1962).
17. The 153rd Committee on Plasma Materials Science, Japan Society for the Promotion of Science, *Plasma Materials Science Handbook* (Ohm corp., Japan, 1992).
18. J. Mostaghimi, M.I. Boulos, Plasma Chem. Plasma Process. **9**, 25 (1989).
19. S.V. Patankar, *Numerical Fluid Flow and Heat Transfer* (Hemisphere, New York, 1980).